

Generation and dynamics of optical beams with polarization singularities

Filippo Cardano¹, Ebrahim Karimi^{1,*}, Lorenzo Marrucci^{1,2}, Corrado de Lisio^{1,2} and Enrico Santamato¹

¹ Dipartimento di Scienze Fisiche, Università di Napoli “Federico II”, Complesso di Monte S. Angelo, 80126 Napoli, Italy

² CNR-SPIN, Complesso Universitario di Monte S. Angelo, 80126 Napoli, Italy

³ CNISM-Conorzio Nazionale Interuniversitario per le Scienze Fisiche della Materia, Napoli, Italy

[Corresponding author: ekarimi@uottawa.ca](mailto:ekarimi@uottawa.ca)

Abstract: We present a convenient method to generate vector beams of light having polarization singularities on their axis, via partial spin-to-orbital angular momentum conversion in a suitably patterned liquid crystal cell. The resulting polarization patterns exhibit a C-point on the beam axis and an L-line loop around it, and may have different geometrical structures such as “lemon”, “star”, and “vortex”. Our generation method allows us to control the radius of L-line loop around the central C-point. Moreover, we investigate the free-air propagation of these fields across a Rayleigh range.

© 2019 Optical Society of America

OCIS codes: 050.4865, 260.6042, 260.5430, 160.3710

References and links

1. J. F. Nye and M. V. Berry, “Dislocations in Wave Trains,” *Proc. R. Soc. Lond. A* **336**, 165–190 (1974).
2. M. R. Dennis, K. O’Holleran, and M. J. Padgett, “Optical Vortices and Polarization Singularities,” *Prog. Opt.* **53**, 293–363 (2009).
3. M. S. Soskin, and M. V. Vasnetsov (Ed. E. Wolf), “Singular optics,” *Prog. Opt.* **42**, 219–276 (2001).
4. S. Franke-Arnold, L. Allen, and M. J. Padgett, “Advances in optical angular momentum,” *Laser Photonics Rev.* **2**, 299313 (2008).
5. J. F. Nye., “Polarization effects in the diffraction of electromagnetic waves: the role of disclinations,” *Proc. Roy. Soc. Lond. A* **387**, 105–132 (1983).
6. J. F. Nye, “Lines of circular polarization in electromagnetic wave fields,” *Proc. Roy. Soc. Lond. A* **389**, 279–290 (1983).
7. M. R. Dennis, “Polarization singularities in paraxial vector fields: morphology and statistics,” *Opt. Commun.* **213**, 201–221 (2002).
8. I. Freund, “Polarization flowers,” *Opt. Commun.* **199**, 47–63 (2001).
9. O. Angelsky, A. Mokhun, I. Mokhun, and M. Soskin, “The relationship between topological characteristics of component vortices and polarization singularities,” *Opt. Commun.* **207**, 57–65 (2002).
10. M. V. Berry, M. R. Dennis, and R. L. Lee Jr., “Polarization singularities in the clear sky,” *New J. Phys.* **6**, 162 (2004).
11. M. S. Soskin, V. Denisenko, and I. Freund, “Optical polarization singularities and elliptic stationary points,” *Opt. Lett.* **28**, 1475–1477 (2003).
12. A. M. Beckley, T. G. Brown, and M. A. Alonso, “Full Poincaré beams,” *Opt. Express* **18**, 10777–10785 (2010).
13. E. J. Galvez, S. Khadka, W. H. Schubert, and S. Nomoto, “Poincaré-beam patterns produced by nonseparable superpositions of Laguerre-Gauss and polarization modes of light,” *Appl. Opt.* **51**, 2925–2934 (2012).
14. L. Marrucci, C. Manzo, and D. Paparo, “Optical Spin-to-Orbital Angular Momentum Conversion in Inhomogeneous Anisotropic Media,” *Phys. Rev. Lett.* **96**, 163905 (2006).
15. A. E. Siegman, *Lasers*, University Science Books (1986).
16. L. Marrucci, E. Karimi, S. Slussarenko, B. Piccirillo, E. Santamato, E. Nagali, and F. Sciarrino, “Spin-to-orbital conversion of the angular momentum of light and its classical and quantum applications,” *J. Opt.* **13**, 064001 (2011).

17. E. Karimi, B. Piccirillo, E. Nagali, L. Marrucci, and E. Santamato, "Efficient generation and sorting of orbital angular momentum eigenmodes of light by thermally tuned q-plates," *Appl. Phys. Lett.* **94**, 231124 (2009).
 18. S. Slussarenko, A. Murauski, T. Du, V. Chigrinov, L. Marrucci, and E. Santamato, "Tunable liquid crystal q-plates with arbitrary topological charge," *Opt. Express* **19**, 4085-4090 (2011).
 19. E. Karimi, G. Zito, B. Piccirillo, L. Marrucci, and E. Santamato, "Hypergeometric-Gaussian modes," *Opt. Lett.* **32**, 3053-3055 (2007).
 20. E. Karimi, B. Piccirillo, L. Marrucci, and E. Santamato, "Light propagation in a birefringent plate with topological charge," *Opt. Lett.* **34**, 1225-1227 (2009).
 21. F. Cardano, E. Karimi, S. Slussarenko, L. Marrucci, C. de Lisio, and E. Santamato, "Polarization pattern of vector vortex beams generated by q-plates with different topological charges," *Appl. Opt.* **51**, C1-C6 (2012).
 22. C. Hnatovsky, V. Shvedov, W. Krolikowski, and A. Rode, "Revealing Local Field Structure of Focused Ultrashort Pulses," *Phys. Rev. Lett.* **106**, 123901 (2011).
 23. A. Ambrosio, L. Marrucci, F. Borbone, A. Roviello, and P. Maddalena, "Light-induced spiral mass transport in azo-polymer films under vortex-beam illumination," *Nat. Commun.* **3**, 989 (2012).
-

1. Introduction

It has been widely studied and directly observed that both longitudinal and transverse waves may have structures rich of singular points [1, 2]. Optical light beams with singular scalar and vectorial features received a particular attention [2]. In the scalar case, these singularities in the beam transverse plane are known as "wave dislocations" or "optical vortices" [1, 3]. They correspond to points where the optical field amplitude vanishes and the optical phase becomes undefined. Near the singular point, the optical phase changes continuously with a specific *topological charge*, given by the phase change in units of 2π along a closed path surrounding the singularity [3]. Beams with optical vortices often carry orbital angular momentum (OAM), which is simply proportional to the topological charge when the vortex is located on the beam axis [4].

When also the vectorial nature of the optical field is taken into account, the variety of possible singular points in the transverse plane is increased [5, 6, 7, 8, 9]. In the paraxial approximation, the optical field is purely transverse, i.e. orthogonal to the propagation direction. In each point of the transverse plane, the direction of the electric field changes in time tracing an ellipse, whose ellipticity and orientation define the local "*polarization*" state of the field. The polarization can be also parametrized by introducing the three *reduced Stokes parameters*, s_1 , s_2 and s_3 , or the polar and azimuthal angles of the *Poincaré sphere*. The vector-field singularities form points or lines in the transverse plane where one of the polarization parameters is undefined. Examples are the so-called *C-points* and *L-lines*, where the orientation and the handedness of the polarization ellipse are undefined, respectively [6, 7]. Optical beams exhibiting vector singularities of this kind have been given various names in the literature, such as for example (full)-Poincaré beams [12, 13]. Here, we simply call them "*polarization-singular beams*" (PSB). The PSB may have different transverse polarization patterns, such as "star", "monstar", "lemon", "vortex", "hyperbolic", etc. For instance, star and lemon correspond to polarization patterns having negative and positive half-integer topological index (or charge) ($\eta_s = -1/2$, $\eta_l = +1/2$) in the beam transverse plane, as defined by the variation of the polarization ellipse orientation for a closed path around a C-point. Optical PSB possessing high values of positive and negative topological charge form so-called "polarization flowers" and "hyperbolic webs", respectively [8].

In this paper, we study the generation and propagation dynamics of vectorial polarization singular beams generated by "q-plates" [14], i.e. birefringent liquid crystal cells having a singular pattern of the optical axis. We generate and control beams characterized by lemon, star and vortex polarization patterns having a central C-point, surrounded by circular L-line that separates two regions in the beam transverse plane characterized by opposite polarization handedness. Finally, we analyzed the polarization structures in different longitudinal positions along the

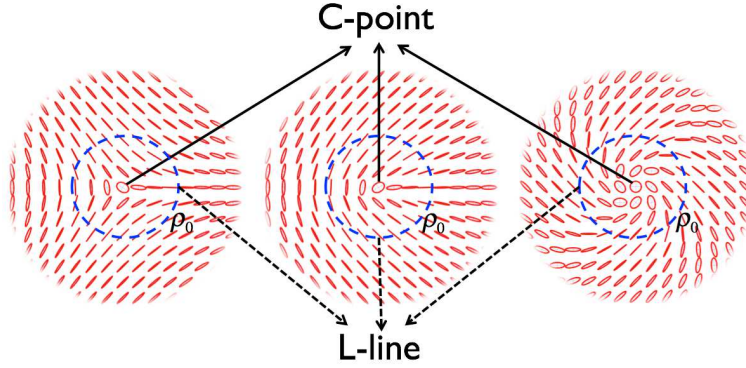


Fig. 1. Polarization patterns of three different polarization singular beams: star ($\eta_s = m/2 = -1/2$), lemon ($\eta_l = m/2 = 1/2$) and vortex ($\eta_v = m/2 = 1$). The central point at the origin indicates the C-point, while dashed blue lines show the L-line circles with radius ρ_0 . The handednesses of the polarization ellipses in the outer region, $\rho > \rho_0$, and in the inner one, $\rho < \rho_0$, are opposite.

beam, to investigate the effect of propagation.

2. Polarization singular beams

A class of polarization singular beams can be generated by the superposition of two optical fields bearing orthogonal polarization states and different OAM values. Here, we consider in particular a beam described by the following expression:

$$|\text{PSB}\rangle = \cos\left(\frac{\delta}{2}\right) \text{LG}_{0,0}(\rho, \phi, z) |L\rangle + e^{i\alpha} \sin\left(\frac{\delta}{2}\right) \text{LG}_{0,m}(\rho, \phi, z) |R\rangle \quad (1)$$

where ρ, ϕ, z are cylindrical coordinates, δ is a tuning parameter, $|L\rangle$ and $|R\rangle$ stand for left- and right-circular polarizations, respectively, α is a phase, and $\text{LG}_{p,m}$ denotes a Laguerre-Gauss mode of radial index p and OAM index m , with a given waist location ($z = 0$) and radius w_0 [15]. The LG modes with non-zero winding number, i.e. $m \neq 0$, have a doughnut shape, with vanishing intensity at the center. The PSB resulting from Eq. (1) have a polarization pattern, shown in Fig. 1, characterized by the following four elements: (i) at the center (that is the beam axis), the polarization is left-circular (C-point), since the last term in Eq. (1) vanishes here; (ii) as the radius increases, the second term contributes and changes the circular polarizations into left-hand elliptical; (iii) at a certain radius $\rho = \rho_0(\delta)$, where the two waves Eq. (1) have equal amplitude, the polarization becomes exactly linear (L-lines); (iv) at larger radii, that is for $\rho > \rho_0$, the second term in Eq. (1) prevails and the polarization state changes into right-handed elliptical. At the C-point, the Stokes parameter s_3 is well-defined, while the azimuthal angle in the Poincaré sphere (or the ellipse orientation) is undefined. Along the L-lines, the polarization state lies on the Poincaré's equator and $s_3 = 0$. It is worth noting that, in this case, the polarization patterns possesses half of the topological charge of the second term in Eq. (1), i.e. $\eta = m/2$. The initial angle at azimuthal location $\phi = 0$ of the polarization ellipse major axis is fixed by the relative phase α in Eq. (1).

We generate PSBs by exploiting partial spin-to-orbital angular momentum conversion in q-plates. The optical action of q-plates is described in [14, 16, 17, 18]. Depending on its birefringent retardation δ , the q-plate converts a varying fraction of the spin angular momentum change suffered by the light passing through the device into OAM with $m = \pm 2q$, where q

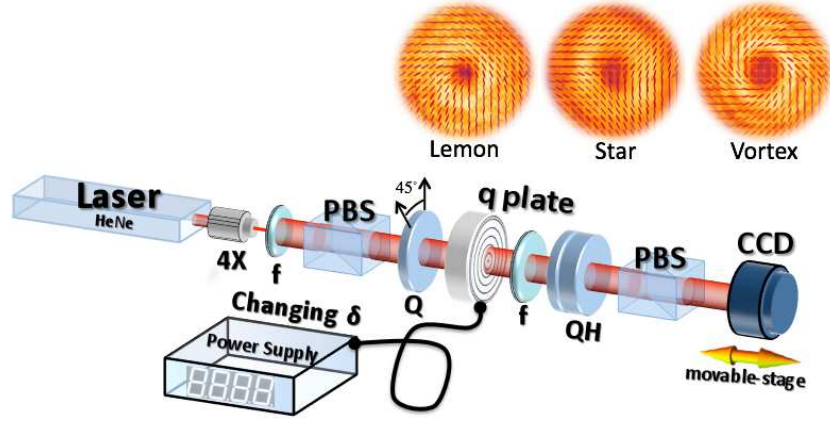


Fig. 2. Layout of the experiment. A He-Ne laser beam was spatially cleaned and linearly polarized. Then, a quarter-wave plate turns the polarization into left-circular (or right-circular). The untuned q-plate then transforms the circular-polarized Gaussian light beam into a PSB. The PSB polarization pattern was then analyzed by a quarter-wave-plate, a half-wave-plate and another polarizer, followed by imaging on a CCD camera. In order to study the propagation dynamics of the PSBs, the CCD camera was mounted on a translation stage and moved around the focal plane of an output lens. Upper insets show the intensity and reconstructed polarization patterns of lemon, star, and vortex beams generated by different q-plates with $q = 1/2, -1/2, 1$, respectively, in the near field just beyond the q-plate. Legend: 4X- microscope objective of 4X, f-lens, PBS- polarizing beam splitter, Q- quarter-wave plate, H- half-wave plate, CCD- charge coupled device.

is the q-plate topological charge and the sign is determined by the input circular polarization handedness. The conversion is full when the q-plate optical phase retardation is $\delta = \pi$ (or any odd multiple of π). For other values of δ , the q-plate is said to be untuned and the spin-to-orbital conversion is only partial. In the untuned q-plate a fraction of the incoming beam passes through unchanged. The field at the exit plane of an untuned q-plate for a Gaussian left-circular polarized input beam is given by the following expression:

$$\hat{U} \cdot |L\rangle = \text{HyGG}_{-|q|\sqrt{2}, q\sqrt{2}}(\rho, d/\bar{n}) \left[\cos\left(\frac{\delta}{2}\right) |L\rangle + e^{i\alpha} \sin\left(\frac{\delta}{2}\right) |R\rangle e^{2iq\phi} \right], \quad (2)$$

where $\text{HyGG}_{-|q|\sqrt{2}, q\sqrt{2}}$ denotes the amplitude profile of a hypergeometric-Gaussian beam [19], describing with good approximation the output mode profile of a q-plate of charge q , thickness d and average refractive index \bar{n} for a Gaussian input (see Ref. [20] for more details), and the phase α in the second term depends on the initial angle (on the x axis) of the q-plate optical-axis pattern [14, 16]. The converted and non-converted terms in Eq. (2) have a common amplitude profile, which can therefore be factorized in the near field (see insets of Fig. 2). The far-field profiles produced by the converted and non-converted parts of the beam are different, however, because of the presence of OAM in the converted part affects the propagation. The HyGG term appearing in Eq. (2), after multiplication by the phase factor $\exp 2iq\phi$, can be expanded in a series of LG modes [19]. Truncating this expansion to the first useful order, Eq. (2) is reduced to Eq. (1). The optical retardation δ of the q-plate, that is the q-plate tuning, can be adjusted continuously by applying an appropriate alternating voltage [18]. Different polarization topologies can be obtained by using q-plates with different topological charges. In this work, we used topological charges q of $-1/2, +1/2$ and $+1$, generating correspondingly equal topological charges of the polarization pattern.

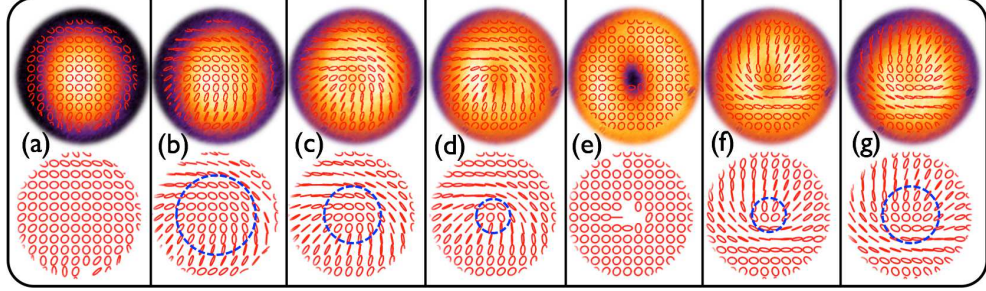


Fig. 3. Intensity distribution and reconstructed polarization patterns of beam generated by a q-plate with $q = 1/2$ for seven different optical retardations: (a) $\delta = 0$ (or 2π), (b) $\delta = \pi/4$, (c) $\delta = \pi/2$, (d) $\delta = 3\pi/4$, (e) $\delta = \pi$, (f) $\delta = 5\pi/4$, and (g) $\delta = 3\pi/2$.

3. Experiment

In our experiment, the beam from a He-Ne laser ($\lambda = 632.8$ nm, 10 mW) was spatially cleaned by focusing it by means of a 4X-microscope objective into a $50 \mu\text{m}$ pinhole and recollimated by a lens of focal length $f = 15$ cm. The beam polarization was then set to left-circular by a polarizing beam splitter (PBS) and a 45° -rotated quarter-wave plate. The beam was then sent into an electrically tunable q-plate, to obtain the entangled spin-orbit state given by Eq. 2. In order to reduce the near-field effects due to radial profiles of converted and non-converted beam, the generated PSB polarization distribution was studied in the focal plane of a convex lens (far-field image). The far-field beam polarization distribution was analyzed by polarization tomography; the local Stokes parameters have been calculated from the intensity images taken by a CCD camera (Sony AS-638CL), after projection onto horizontal (H), vertical (V), anti-diagonal (A), diagonal (D), L and R polarization states, respectively. The far-field polarization pattern was thus entirely reconstructed, as is shown in form of little ellipses in Fig. 2 and subsequent figures. In order to reduce noise and experimental errors, the average intensity was recorded in a grid of 20×20 pixel square area [21]. The missing ellipses in the experimentally reconstructed polarization patterns (e.g., in Fig. 3) correspond to regions with low intensity, so that the polarization reconstruction was affected by stray light. The superposition coefficients in Eq. (2) have been adjusted by changing the q-plate optical retardation δ by the applied voltage. The radius where the L-line forms in the polarization pattern depends on the ratio between the absolute value of the two coefficients in Eq. (2) and, hence, on the voltage applied to the q-plate. In particular, for optical retardation $\delta = 0$ and $\delta = \pi$ the far-field beam profile is Gaussian fully right-circular and doughnut-shaped fully left-circular, respectively. In the intermediate case, the pattern is a superposition and a circular L-line appears in the polarization pattern, whose radius depends on the δ value. Figure (3) shows the intensity and reconstructed polarization pattern for different q-plate retardations in steps $\Delta\delta = \pi/4$. As shown in the figure, also the intensity profile changes from Gaussian (left-circular) to doughnut (right-circular) shape. In Fig. 3 (c) and (g), the optical retardations are $\pi/2$ and $3\pi/2$, respectively; the π difference in the relative phase appears as an 180° rotation of the polarization pattern. The topological charge of the polarization pattern, however, depends only on the q -value of the q-plate, and in the case of Fig. 3 we have $q = \eta = 1/2$.

In a second experiment, we studied the dynamics of different PSBs with $\eta = -1/2$, $+1/2$ and $+1$ topologies under free-air propagation for fixed optical retardation $\pi/2$ of the q-plate. The beam emerging from the q-plate was focused by a lens and a moving system made of CCD camera and 4X microscope objective was used to record the beam intensity and polarization features at six different planes in the range $-z_R \leq z \leq z_R$, where z_R is the lens Rayleigh param-

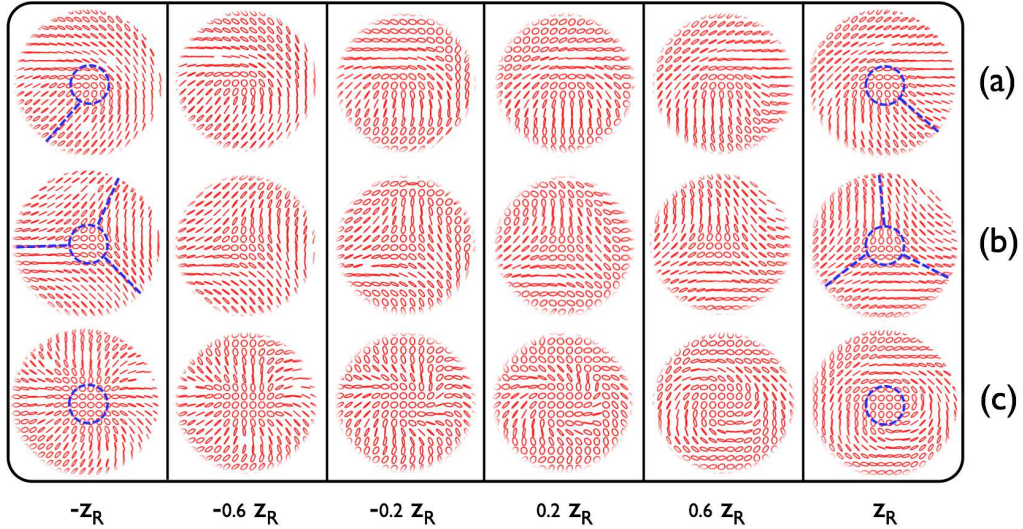


Fig. 4. Reconstructed experimental polarization patterns of different PSB beams. (a) $\eta = m/2 = +1/2$, (b) $\eta = m/2 = -1/2$ and (c) $\eta = m/2 = +1$. Patterns have been reconstructed by measuring the maps of reduced Stokes parameters in six different longitudinal planes within the beam Rayleigh range, from $-z_R$ to $+z_R$.

eter and $z = 0$ corresponds to the beam waist location. The experimental results are shown in Fig. 4. As it can be seen, the polarization pattern evolves during propagation. Indeed LG_{00} and $LG_{0,m}$ modes of Eq. (1) have different z dependences of their Gouy phases; the relative phase between them is given by $\exp(i|m|\arctan(z/z_0))$, which in the explored region varies in the range $|m|[-\pi/4, \pi/4]$. In the case $m = \pm 1$ the phase evolution leads to a simple rotation of the whole polarization structure (as in Fig. 4 (a) and (b)), while when $m = 2$ this dephasing leads to more interesting pattern dynamics, in which the polarization structure changes from radial-like to vortex and then to an azimuthal-like pattern (Fig. 4 (c)).

4. Conclusion

We reported a novel and simple non-interferometric technique to generate beams carrying a polarization singularity on its axis based on a partial spin-to-orbital angular momentum conversion in a detuned q-plate device. By this approach, we generated beams with C-points on the optical axis, surrounded by a circular L-lines whose radius was controlled by the voltage applied to the q-plate, and having different patterns such as lemons, stars and vortices, corresponding to vector topological charges of $-1/2$, $1/2$ and $+1$. We have also studied the pattern evolution in free-space propagation. Such polarization patterns could find practical application in lithographic optical techniques, as for the examples discussed in Refs. [22, 23].

Acknowledgments

We thank Sergei Slussarenko for preparing the q-plates. We acknowledge financial support of the Future and Emerging Technologies FET-Open programme, within the 7th Framework Programme for Research of the European Commission, under grant number 255914 - PHOR-BITECH.